

# Todo list

Write acknowledgements . . . . .	v
Write overview . . . . .	4
Add off-peak analysis! . . . . .	130
Here we need to cite Mattana et al. (2009). . . . .	144
Next, we will discuss Figure 9.2... . . . .	144
Next, we will discuss Figure 9.3... . . . .	144
What would make good future work. Something about CTA population study, something about improved modeling liek HESS J1825, something about better PSF . . . . .	147

NEUTRON STAR POWERED NEBULAE: A NEW VIEW ON  
PULSAR WIND NEBULAE WITH THE FERMI GAMMA-RAY  
SPACE TELESCOPE

A DISSERTATION  
SUBMITTED TO THE DEPARTMENT OF PHYSICS  
AND THE COMMITTEE ON GRADUATE STUDIES  
OF STANFORD UNIVERSITY  
IN PARTIAL FULFILLMENT OF THE REQUIREMENTS  
FOR THE DEGREE OF  
DOCTOR OF PHILOSOPHY

Joshua Jeremy Lande

April 2013

© Copyright by Joshua Jeremy Lande 2013  
All Rights Reserved

I certify that I have read this dissertation and that, in my opinion, it is fully adequate in scope and quality as a dissertation for the degree of Doctor of Philosophy.

---

(Stefan Funk) Principal Adviser

I certify that I have read this dissertation and that, in my opinion, it is fully adequate in scope and quality as a dissertation for the degree of Doctor of Philosophy.

---

(Elliott Bloom)

I certify that I have read this dissertation and that, in my opinion, it is fully adequate in scope and quality as a dissertation for the degree of Doctor of Philosophy.

---

(Roger Romani)

Approved for the University Committee on Graduate Studies

# Contents

<b>Abstract</b>	<b>iv</b>
<b>Acknowledgement</b>	<b>v</b>
<b>1 Overview</b>	<b>4</b>
<b>2 Gamma-ray Astrophysics</b>	<b>5</b>
2.1 Astronomy and the Atmosphere . . . . .	5
2.2 The History of Gamma-ray Astrophysics . . . . .	6
2.3 The <i>Fermi</i> Gamma-ray Space Telescope . . . . .	14
2.3.1 The LAT Detector . . . . .	15
2.3.2 Performance of the LAT . . . . .	15
2.4 Pulsars and Pulsar Wind Nebulae . . . . .	16
2.4.1 Pulsars . . . . .	16
2.4.2 Pulsar Wind Nebulae . . . . .	19
2.5 Sources Detected by the Large Area Telescope . . . . .	21
2.5.1 The Galactic Diffuse and Isotropic Gamma-ray Background .	23
2.5.2 The Second Fermi Catalog . . . . .	24
2.5.3 The Second Fermi Pulsar Catalog . . . . .	24
2.5.4 Pulsar Wind Nebulae Detected by the Large Area Telescope .	25
2.6 Radiation Processes in Gamma-ray Astrophysics . . . . .	29
2.6.1 Synchrotron . . . . .	29
2.6.2 Inverse Compton . . . . .	31
2.6.3 Bremsstrahlung . . . . .	32

2.6.4	Pion Decay . . . . .	33
<b>3</b>	<b>The Pulsar/Pulsar Wind Nebula System</b>	<b>34</b>
3.1	Neutron Star Formation . . . . .	34
3.2	Pulsar Evolution . . . . .	35
3.3	Pulsar Magnetosphere . . . . .	39
3.4	Pulsar Wind Nebulae Structure . . . . .	40
3.5	Pulsar Wind Nebula Emission . . . . .	41
<b>4</b>	<b>Maximum-likelihood analysis of LAT data</b>	<b>46</b>
4.1	Motivations for Maximum-Likelihood Analysis of Gamma-ray Data .	47
4.2	Description of Maximum-Likelihood Analysis . . . . .	48
4.3	Defining a Model of the Sources in the Sky . . . . .	49
4.4	The LAT Instrument Response Functions . . . . .	51
4.5	Binned Maximum-Likelihood of LAT Data with the Science Tools . .	53
4.6	The Alternate Maximum-Likelihood Package <code>pointlike</code> . . . . .	55
<b>5</b>	<b>Analysis of Spatially Extended LAT Sources</b>	<b>57</b>
5.1	Introduction . . . . .	57
5.2	Analysis Method . . . . .	60
5.2.1	Modeling Extended Sources in the <code>pointlike</code> Package . . . . .	60
5.2.2	Extension Fitting . . . . .	61
5.2.3	<code>gtlike</code> Analysis Validation . . . . .	65
5.2.4	Comparing Source Sizes . . . . .	65
5.3	Validation of the TS Distribution . . . . .	67
5.3.1	Point-like Source Simulations Over a Uniform Background . .	67
5.3.2	Point-like Source Simulations Over a Structured Background .	72
5.3.3	Extended Source Simulations Over a Structured Background .	73
5.4	Extended Source Detection Threshold . . . . .	75
5.5	Testing Against Source Confusion . . . . .	82
5.6	Test of 2LAC Sources . . . . .	89

<b>6</b>	<b>Search for Spatially-extended LAT Sources</b>	<b>92</b>
6.1	Analysis of Extended Sources Identified in the 2FGL Catalog . . . . .	93
6.2	Systematic Errors on Extension . . . . .	94
6.3	Extended Source Search Method . . . . .	97
6.4	New Extended Sources . . . . .	103
6.4.1	2FGL J0823.0–4246 . . . . .	106
6.4.2	2FGL J0851.7–4635 . . . . .	108
6.4.3	2FGL J1615.0–5051 . . . . .	108
6.4.4	2FGL J1615.2–5138 . . . . .	112
6.4.5	2FGL J1627.0–2425c . . . . .	113
6.4.6	2FGL J1632.4–4753c . . . . .	114
6.4.7	2FGL J1712.4–3941 . . . . .	117
6.4.8	2FGL J1837.3–0700c . . . . .	119
6.4.9	2FGL J2021.5+4026 . . . . .	121
6.5	Discussion . . . . .	124
<b>7</b>	<b>Search for PWNe associated with Gamma-loud Pulsars</b>	<b>130</b>
7.1	Off-peak Phase Selection . . . . .	130
7.2	Off-peak Analysis Method . . . . .	130
7.3	Off-peak Results . . . . .	130
7.4	Off-Peak Individual Source Discussion . . . . .	130
<b>8</b>	<b>Search for PWNe associated with TeV Pulsars</b>	<b>131</b>
8.1	Introduction . . . . .	132
8.2	List of very high energy (VHE) PWN Candidates . . . . .	132
8.3	Analysis Method . . . . .	135
8.4	Sources Detected . . . . .	137
8.4.1	“PWN”-type and “PWNe”-type Sources . . . . .	138
8.4.2	“O”-type Sources . . . . .	140
8.4.3	“PSR”-type Sources . . . . .	140
<b>9</b>	<b>Population Study of LAT-detected PWNe</b>	<b>141</b>

## 10 Future Work (or Outlook)

147



# List of Tables

5.1	Monte Carlo Spectral Parameters . . . . .	71
5.2	Extension Detection Threshold . . . . .	80
6.1	Analysis of the twelve extended sources included in the 2FGL catalog	95
6.2	Nearby Residual-induced Sources . . . . .	102
6.3	Extension fit for the nine additional extended sources . . . . .	104
6.4	Dual localization, alternative PSF, and alternative approach to modeling the diffuse emission . . . . .	105
8.1	List of analyzed VHE sources . . . . .	133
8.1	List of analyzed VHE sources . . . . .	134
8.2	Spatial and spectral results for detected VHE sources . . . . .	137
9.1	The muliwavelenth properties of the VHE source and their associated the Large Area Telescope (LAT)-detected pulsars. . . . .	142

# List of Figures

2.1	Transparency of the atmosphere of the earth to photons of varying wavelenthts. This figure is from Carroll & Ostlie (2006)	6
2.2	The experimental design of Explorer XI. This figure is from Kraushaar et al. (1965).	8
2.3	The position of all 621 cosmic $\gamma$ -rays detected by the Third Orbiting Solar Observatory (OSO-3). This figure is from Kraushaar et al. (1972).	9
2.4	A map of the sources observed by COS-B. The filled circles represent brighter sources. The unshaded region corresponds to the parts of the sky observed by COS-B. This figure is from Swanenburg et al. (1981).	11
2.5	A diagram of the the Energetic Gamma Ray Experiment Telescope (EGRET) detector. This figure is from (Thompson et al. 1993).	12
2.6	The position of EGRET sources in the sky in galactic coordinates. The size of the source markers corresponds to the overall source intensity. This figure is from (Hartman et al. 1999).	13
2.7	A schematic diagram of the LAT with an incident $\gamma$ -ray (red line) pair-converting into an electron and positron (blue lines) which are recorded in the tracker and calorimeter of the LAT. This figure is taken from (Atwood et al. 2009). This diagram shows the three major subsystems of the LAT: the tracker, the calorimeter, and the Anti-Coincidence Detector (ACD).	14
2.8	The LAT point-source sensitivity for exposures of 100 s, 1 orbit, 1 day, and 1 yr. This figure is from Atwood et al. (2009).	16

2.9	The LAT effective area (a) as a function of energy for $\gamma$ -rays that are incident on the LAT perpendicularly from above and (b) as a function of incident angle for photons with an energy of 10 GeV. The LAT performance is computed for the <b>P7SOURCE_V6</b> event classification. This figure is from Ackermann et al. (2012). . . . .	17
2.10	The angular resolution (68% and 95% containment radius) as a function of energy. The LAT performance is computed for the <b>P7SOURCE_V6</b> event classification. This figure is from Ackermann et al. (2012). . .	17
2.11	The energy dispersion (a) as a function of energy for $\gamma$ -rays that are incident on the LAT perpendicularly from above and (b) as a function of the incident angle for photons with an energy of 10 GeV. The LAT performance is computed for the <b>P7SOURCE_V6</b> event classification. This figure is from Ackermann et al. (2012). . . . .	18
2.12	The Orion plate from Bevis' book <i>Uranographia Britannica</i> . The Crab nebula can be found on the horn of Taurus the Bull on the top of the figure and the source is marked by a cloudy symbol. This figure was reproduced from Ashworth (1981). . . . .	20
2.13	An Aitoff projection map of the $\gamma$ -ray sky observed by the LAT with a 2 years exposure. This map is integrated in the energy range from 100 MeV to 10 GeV in units of $10^{-7}\text{erg cm}^{-2}\text{s}^{-1}\text{sr}^{-1}$ . This figure is from Nolan et al. (2012). . . . .	22
2.14	The spectral energy distribution (SED) of the Crab nebula observed by the LAT as well as a variety of other instruments. This figure is from Abdo et al. (2010e). . . . .	26
2.15	The SED of Vela-X observed at radio, x-ray, $\gamma$ -ray, and VHE energies. The emission was suggested by (Abdo et al. 2010) to be driven by two populations of electrons. In this model, the lower-energy electron population powers the radio and $\gamma$ -ray emission and the higher-energy electron population powers the x-ray and VHE emission. This figure is from Abdo et al. (2010). . . . .	27

2.16	In synchrotron radiation, charged particles spiral along magnetic field lines, radiating photons as they accelerate. . . . .	29
3.1	The rotating dipole model of a pulsar. This figure is taken from (Carroll & Ostlie 2006). . . . .	36
3.2	The magnetosphere for a rotating pulsar. The pulsar is on the bottom left of the plot. This figure is from Goldreich & Julian (1969). . . . .	40
3.3	The regions of emission in a pulsar/pulsar wind nebula (PWN) system. This figure shows (top) the pulsar's magnetosphere, (middle), the unshocked pulsar wind and (bottom) the shocked pulsar wind which can be observed as the PWN. "R", "O", "X", and " $\gamma$ " describe sites of radio, optical, X-ray, and $\gamma$ -ray emission respectively. "CR", "Sy", and "IC" refer to regions of curvature, inverse Compton, and synchrotron emission. Figure is taken from Aharonian & Bogovalov (2003). . . . .	42
5.1	Counts maps and TS profiles for the SNR IC 443. (a) TS vs. extension of the source. (b) $TS_{\text{ext}}$ for individual energy bands. (c) observed radial profile of counts in comparison to the expected profiles for a spatially extended source (solid and colored red in the online version) and for a point-like source (dashed and colored blue in the online version). (d) smoothed counts map after subtraction of the diffuse emission compared to the smoothed LAT PSF (inset). Both were smoothed by a $0.1^\circ$ 2D Gaussian kernel. Plots (a), (c), and (d) use only photons with energies between 1 GeV and 100 GeV. Plots (c) and (d) include only photons which converted in the front part of the tracker and have an improved angular resolution (Atwood et al. 2009). . . . .	64

5.2	A comparison of a 2D Gaussian and uniform disk spatial model of extended sources before and after convolving with the PSF for two energy ranges. The solid black line is the PSF that would be observed for a power-law source of spectral index 2. The dashed line and the dash-dotted lines are the brightness profile of a Gaussian with $r_{68} = 0.5$ and the convolution of this profile with the LAT PSF respectively (colored red in the online version). The dash-dot-dotted and the dot-dotted lines are the brightness profile of a uniform disk with $r_{68} = 0.5$ and the convolution of this profile with the LAT PSF respectively (colored blue in the online version). . . . .	66
5.3	Cumulative distribution of the TS for the extension test when fitting simulated point-like sources in the 1 GeV to 100 GeV energy range. The four plots represent simulated sources of different spectral indices and the different lines (colored in the online version) represent point-like sources with different 100 MeV to 100 GeV integral fluxes. The dashed line (colored red) is the cumulative density function of Equation 5.11. . . . .	69
5.4	The same plot as Figure 5.3 but fitting in the 10 GeV to 100 GeV energy range. . . . .	70
5.5	Cumulative distribution of $TS_{\text{ext}}$ for sources simulated on top of the Galactic diffuse and isotropic background. . . . .	74
5.6	The distribution of TS values when fitting 985 statistically independent simulations of W44. (a) is the distribution of TS values when fitting W44 as a point-like source and (b) is the distribution of $TS_{\text{ext}}$ when fitting the source with a uniform disk or a radially-symmetric Gaussian spatial model. (c) is the distribution of the change in TS when fitting the source with an elliptical disk spatial model compared to fitting it with a radially-symmetric disk spatial model and (d) when fitting the source with an elliptical ring spatial model compared to an elliptical disk spatial model. . . . .	76

5.7	The distribution of fit parameters for the Monte Carlo simulations of W44. The plots show the distribution of best fit (a) flux (b) spectral index and (c) 68% containment radius. The dashed vertical lines represent the simulated values of the parameters. . . . .	77
5.8	The detection threshold to resolve an extended source with a uniform disk model for a two-year exposure. All sources have an assumed power-law spectrum and the different line styles (colors in the electronic version) correspond to different simulated spectral indices. The lines with no markers correspond to the detection threshold using photons with energies between 100 MeV and 100 GeV, while the lines with star-shaped markers correspond to the threshold using photons with energies between 1 GeV and 100 GeV. . . . .	79
5.9	The LAT detection threshold for four spectral indices and three backgrounds ( $1\times$ , $10\times$ , and $100\times$ the Sreekumar-like isotropic background) for a two-year exposure. The left-hand plots are the detection threshold when using photons with energies between 1 GeV and 100 GeV and the right-hand plots are the detection threshold when using photons with energies between 10 GeV and 100 GeV. The flux is integrated only in the selected energy range. Overlaid on this plot are the LAT-detected extended sources placed by the magnitude of the nearby Galactic diffuse emission and the energy range they were analyzed with. The star-shaped markers (colored red in the electronic version) are sources with a spectral index closer to 1.5, the triangular markers (colored blue) an index closer to 2, and the circular markers (colored green) an index closer to 2.5. The triangular marker in plot (d) below the sensitivity line is MSH 15–52. . . . .	81

5.10	The projected detection threshold of the LAT to extension after 10 years for a power-law source of spectral index 2 against 10 times the isotropic background in the energy range from 1 GeV to 100 GeV (solid line colored red in the electronic version) and 10 GeV to 100 GeV (dashed line colored blue). The shaded gray regions represent the detection threshold assuming the sensitivity improves from 2 to 10 years by the square root of the exposure (top edge) and linearly with exposure (bottom edge). The lower plot shows the factor increase in sensitivity. For small extended sources, the detection threshold of the LAT to the extension of a source will improve by a factor larger than the square root of the exposure. . . . .	83
5.11	(a) and (b) are the distribution of $TS_{\text{ext}}$ and of $TS_{2\text{pts}}$ when fitting simulated spatially extended sources of varying sizes as both an extended source and as two point-like sources. (c) and (d) are the distribution of $TS_{\text{ext}} - TS_{2\text{pts}}$ for the same simulated sources. (a) and (c) represent sources fit in the 1 GeV to 100 GeV energy range and (b) and (d) represent sources fit in the 10 GeV to 100 GeV energy range. In (c) and (d), the plus-shaped markers (colored red in the electronic version) are fits where $TS_{\text{ext}} \geq 16$ . . . . .	86
5.12	The distribution of $TS_{\text{ext}} - TS_{2\text{pts}}$ when fitting two simulated point-like sources of varying separations as both an extended source and as two point-like sources. (a), and (b) represent simulations of two point-like sources with the same spectral index and (c) and (d) represent simulations of two point-like sources with different spectral indices. (a) and (c) fit the simulated sources in the 1 GeV to 100 GeV energy range and (b) and (d) fit in the 10 GeV to 100 GeV energy range. The plus-shaped markers (colored red in the electronic version) are fits where $TS_{\text{ext}} \geq 16$ . . . . .	87

5.13	The cumulative density of $TS_{\text{ext}}$ for the 733 clean AGN in 2LAC that were significant above 1 GeV calculated with <code>pointlike</code> (dashed line colored blue in the electronic version) and with <code>gtlike</code> (solid line colored black). AGN are too far and too small to be resolved by the LAT. Therefore, the cumulative density of $TS_{\text{ext}}$ is expected to follow a $\chi^2_1/2$ distribution (Equation 5.11, the dash-dotted line colored red). . . . .	91
6.1	A TS map generated for the region around the SNR IC 443 using photons with energies between 1 GeV and 100 GeV. (a) TS map after subtracting IC 443 modeled as a point-like source. (b) same as (a), but IC 443 modeled as an extended source. The cross represents the best fit position of IC 443. . . . .	99
6.2	A diffuse-emission-subtracted 1 GeV to 100 GeV counts map of the region around 2FGL J1856.2+0450c smoothed by a $0^\circ.1$ 2D Gaussian kernel. The plus-shaped marker and circle (colored red in the online version) represent the center and size of the source fit with a radially-symmetric uniform disk spatial model. The black crosses represent the positions of other 2FGL sources. The extension is statistically significant, but the extension encompasses many 2FGL sources and the emission does not look to be uniform. Although the fit is statistically significant, it likely corresponds to residual features of inaccurately modeled diffuse emission picked up by the fit. . . . .	101



- 6.3 A diffuse-emission-subtracted 1 GeV to 100 GeV counts map of 2FGL J0823.0–4246 smoothed by a  $0^{\circ}.1$  2D Gaussian kernel. The triangular marker (colored red in the online version) represents the 2FGL position of this source. The plus-shaped marker and the circle (colored red) represent the best fit position and extension of this source assuming a radially-symmetric uniform disk model. The two star-shaped markers (colored green) represent 2FGL sources that were removed from the background model. From left to right, these sources are 2FGL J0823.4–4305 and 2FGL J0821.0–4254. The lower right inset is the model predicted emission from a point-like source with the same spectrum as 2FGL J0823.4–4305 smoothed by the same kernel. This source is spatially coincident with the Puppis A SNR. The light blue contours correspond to the X-ray image of Puppis A observed by *ROSAT* (Petre et al. 1996). . . . . 107
- 6.4 A diffuse-emission-subtracted 10 GeV to 100 GeV counts map of 2FGL J0851.7–4635 smoothed by a  $0^{\circ}.25$  2D Gaussian kernel. The triangular marker (colored red in the electronic version) represents the 2FGL position of this source. The plus-shaped marker and the circle (colored red) are the best fit position and extension of this source assuming a radially-symmetric uniform disk model. The three black crosses represent background 2FGL sources. The three star-shaped markers (colored green) represent other 2FGL sources that were removed from the background model. They are (from left to right) 2FGL J0853.5–4711, 2FGL J0855.4–4625, and 2FGL J0848.5–4535. The circular and square-shaped marker (colored blue) represents the 2FGL and relocalized position of another 2FGL source. This extended source is spatially coincident with the Vela Jr. SNR. The contours (colored light blue) correspond to the TeV image of Vela Jr. (Aharonian et al. 2007c). . . 109

- 6.5 A diffuse-emission-subtracted 10 GeV to 100 GeV counts map of 2FGL J1615.0–5051 (upper left) and 2FGL J1615.2–5138 (lower right) smoothed by a  $0^\circ.1$  2D Gaussian kernel. The triangular markers (colored red in the electronic version) represent the 2FGL positions of these sources. The cross-shaped markers and the circles (colored red) represent the best fit positions and extensions of these sources assuming a radially symmetric uniform disk model. The two black crosses represent background 2FGL sources and the star-shaped marker (colored green) represents 2FGL J1614.9-5212, another 2FGL source that was removed from the background model. The contours (colored light blue) correspond to the TeV image of HESS J1616–508 (left) and HESS J1614–518 (right) (Aharonian et al. 2006e). . . . . 110
- 6.6 A diffuse-emission-subtracted 1 GeV to 100 GeV counts map of (a) the region around 2FGL J1627.0–2425 smoothed by a  $0^\circ.1$  2D Gaussian kernel and (b) with the emission from 2FGL J1625.7–2526 subtracted. The triangular marker (colored red in the online version) represents the 2FGL position of this source. The plus-shaped marker and the circle (colored red) represent the best fit position and extension of this source assuming a radially-symmetric uniform disk model and the black cross represents a background 2FGL source. The contours in (a) correspond to the  $100\ \mu\text{m}$  image observed by IRAS (Young et al. 1986). The contours in (b) correspond to CO ( $J = 1 \rightarrow 0$ ) emission integrated from  $-8\ \text{km s}^{-1}$  to  $20\ \text{km s}^{-1}$ . They are from de Geus et al. (1990), were cleaned using the moment-masking technique (Dame 2011), and have been smoothed by a  $0^\circ.25$  2D Gaussian kernel. . . . . 113

- 6.7 A diffuse-emission-subtracted 10 GeV to 100 GeV counts map of 2FGL J1632.4–4753c (a) smoothed by a  $0^\circ.1$  2D Gaussian kernel and (b) with the emission from the background sources subtracted. The triangular marker (colored red in the electronic version) represents the 2FGL position of this source. The plus-shaped marker and the circle (colored red) are the best fit position and extension of 2FGL J1632.4–4753c assuming a radially-symmetric uniform disk model. The four black crosses represent background 2FGL sources subtracted in (b). The circular and square-shaped markers (colored blue) represent the 2FGL and relocalized positions respectively of two additional background 2FGL sources subtracted in (b). The star-shaped marker (colored green) represents 2FGL J1634.4–4743c, another 2FGL source that was removed from the background model. The contours (colored light blue) correspond to the TeV image of HESS J1632–478 (Aharonian et al. 2006e). . . . 115
- 6.8 The spectral energy distribution of four extended sources associated with unidentified extended TeV sources. The black points with circular markers are obtained by the LAT. The points with plus-shaped markers (colored red in the electronic version) are for the associated the High Energy Stereoscopic System (H.E.S.S.) sources. (a) the LAT SED of 2FGL J1615.0–5051 together with the H.E.S.S. SED of HESS J1616–508. (b) 2FGL J1615.2–5138 and HESS J1614–518. (c) 2FGL J1632.4–4753c and HESS J1632–478. (d) 2FGL J1837.3–0700c and HESS J1837–069. The H.E.S.S. data points are from (Aharonian et al. 2006e). Both LAT and H.E.S.S. spectral errors are statistical only. . . . . 116

6.9	A diffuse-emission-subtracted 10 GeV to 100 GeV counts map of 2FGL J1712.4–3941 (a) smoothed by a $0^\circ.15$ 2D Gaussian kernel and (b) with the emission from the background sources subtracted. This source is spatially coincident with RX J1713.7–3946 and was recently studied in Abdo et al. (2011b). The triangular marker (colored red in the online version) represents the 2FGL position of this source. The plus-shaped marker and the circle (colored red) are the best fit position and extension of this source assuming a radially symmetric uniform disk model. The two black crosses represent background 2FGL sources subtracted in (b). The contours (colored light blue) correspond to the TeV image (Aharonian et al. 2007d).	118
6.10	A diffuse-emission-subtracted 10 GeV to 100 GeV counts map of the region around 2FGL J1837.3–0700c (a) smoothed by a $0^\circ.15$ 2D Gaussian kernel and (b) with the emission from the background sources subtracted. The triangular marker (colored red in the online version) represents the 2FGL position of this source. The plus-shaped marker and the circle (colored red) represent the best fit position and extension of 2FGL J1837.3–0700c assuming a radially-symmetric uniform disk model. The circular and square-shaped markers (colored blue) represent the 2FGL and the relocalized positions respectively of two background 2FGL sources subtracted in (b). The star-shaped marker (colored green) represents 2FGL J1835.5–0649, another 2FGL source that was removed from the background model. The contours (colored light blue) correspond to the TeV image of HESS J1837–069 (Aharonian et al. 2006e). The diamond-shaped marker (colored orange) represents the position of PSR J1838–0655 and the hexagonal-shaped marker (colored purple) represents the position AX J1837.3–0652 (Gotthelf & Halpern 2008).	120

- 6.11 A diffuse-emission-subtracted 10 GeV to 100 GeV counts map of the region around 2FGL J2021.5+4026 smoothed by a  $0.1^\circ$  2D Gaussian kernel. The triangular marker (colored red in the online version) represents the 2FGL position of this source. The plus-shaped marker and the circle (colored red) represent the best fit position and extension of 2FGL J2021.5+4026 assuming a radially-symmetric uniform disk model. The star-shaped marker (colored green) represents 2FGL J2019.1+4040, a 2FGL source that was removed from the background model. 2FGL J2021.5+4026 is spatially coincident with the  $\gamma$ -Cygni SNR. The contours (colored light blue) correspond to the 408MHz image of  $\gamma$ -Cygni observed by the Canadian Galactic Plane Survey (Taylor et al. 2003). . . . . 122
- 6.12 The spectral energy distribution of the extended sources Puppis A (2FGL J0823.0–4246) and  $\gamma$ -Cygni (2FGL J2021.5+4026). The lines (colored red in the online version) are the best fit power-law spectral models of these sources. Puppis A has a spectral index of  $2.21 \pm 0.09$  and  $\gamma$ -Cygni has an index of  $2.42 \pm 0.19$ . The spectral errors are statistical only. The upper limit is at the 95% confidence level. . . . 123
- 6.13 The 21 spatially extended sources detected by the LAT at GeV energies with 2 years of data. The twelve extended sources included in 2FGL are represented by the circular markers (colored red in the online version). The nine new extended sources are represented by the triangular markers (colored orange). The source positions are overlaid on a 100 MeV to 100 GeV Aitoff projection sky map of the LAT data in Galactic coordinates. . . . . 125

6.14	A comparison of the sizes of extended sources detected at both GeV and TeV energies. The TeV sizes of W30, 2FGL J1837.3–0700c, 2FGL J1632.4–4753c, 2FGL J1615.0–5051, and 2FGL J1615.2–5138 are from Aharonian et al. (2006e). The TeV sizes of MSH 15–52, HESS J1825–137, Vela X, Vela Jr., RX J1713.7–3946 and W28 are from Aharonian et al. (2005a, 2006c,d, 2007c,d, 2008a). The TeV size of IC 443 is from Acciari et al. (2009) and W51C is from Krause et al. (2011). The TeV sizes of MSH 15–52, HESS J1614–518, HESS J1632–478, and HESS J1837–069 have only been reported with an elliptical 2D Gaussian fit and so the plotted sizes are the geometric mean of the semi-major and semi-minor axis. The LAT extension of Vela X is from Abdo et al. (2010). The TeV sources were fit assuming a 2D Gaussian surface brightness profile so the plotted GeV and TeV extensions were first converted to $r_{68}$ (see Section 5.2.4). Because of their large sizes, the shape of RX J1713.7–3946 and Vela Jr. were not directly fit at TeV energies and so are not included in this comparison. On the other hand, dedicated publications by the LAT collaboration on these sources showed that their morphologies are consistent (Abdo et al. 2011b; Tanaka et al. 2011). The LAT extension errors are the statistical and systematic errors added in quadrature. . . . .	126
6.15	The distributions of the sizes of 18 extended LAT sources at GeV energies (colored blue in the electronic version) and the sizes of the 40 extended H.E.S.S. sources at TeV energies (colored red). The H.E.S.S. sources were fit with a 2D Gaussian surface brightness profile so the LAT and H.E.S.S. sizes were first converted to $r_{68}$ . The GeV size of Vela X is taken from Abdo et al. (2010). Because of their large sizes, the shape of RX J1713.7–3946 and Vela Jr. were not directly fit at TeV energies and are not included in this comparison. Centaurus A is not included because of its large size. . . . .	127

6.16	The distribution of spectral indices of the 1873 2FGL sources (colored red in the electronic version) and the 21 spatially extended sources (colored blue). The index of Centaurus A is taken from Nolan et al. (2012) and the index of Vela X is taken from Abdo et al. (2010).	129
9.1	The observed $\gamma$ -ray luminosity compared to the observed spin-down luminosity for all PWN candidates presented in Table 9.1.	143
9.2	...	145
9.3	...	146

# List of Acronyms

- 1FHL** the first *Fermi* hard-source list. 135
- 2CG** the second COS-B catalog. 10
- 2FGL** the second *Fermi* catalog. 23, 24, 47, 131, 136
- 2PC** the second *Fermi* pulsar catalog. 23–25, 133, 134
- 3EG** the Third EGRET Catalog. 12
- ACD** Anti-Coincidence Detector. xii, 14, 15
- AGILE** Astro-rivelatore Gamma a Immagini LEggero. 12, 26
- AGN** active galactic nucleus. 24
- arcsec** second of arc. 41
- ASI** Italian Space Agency. 12
- ATNF** Australia Telescope National Facility. 19
- BPL** broken-power law. 50
- CGRO** the Compton Gamma Ray Observatory. 11
- CGS** the Centimetre-Gram-Second System of Units. 49–51
- CMB** cosmic microwave background. 43



**CsI** cesium iodide. 15

**DOE** United States Department of Energy. 12

**ECPL** exponentially-cutoff power law. 50

**EGRET** the Energetic Gamma Ray Experiment Telescope. xii, 10–13, 19, 25, 48, 55

**ESA** the European Space Agency. 10

**FWHM** full width at half maximum. 9

**GBM** Gamma-ray Burst Monitor. 14

**GRB** gamma-ray burst. 14

**H.E.S.S.** the High Energy Stereoscopic System. xxi, xxiv, 28, 29, 47, 58, 112, 114, 116, 117, 119, 124, 127, 128

**HMB** high-mass binary. 24

**IACT** Imaging air Cherenkov detector. 21, 58, 128, 131, 135

**IC** inverse Compton. 7, 21, 23, 28, 29, 31, 32, 40, 41, 43, 44, 135

**LAT** the Large Area Telescope. iv, v, vii, xi–xiii, 14–18, 22–26, 28, 29, 40, 45, 51–53, 55, 131, 132, 134–137, 140–142, 144

**LMC** Large Magellanic Cloud. 21

**LRT** likelihood-ratio test. 49, 55

**MIT** the Massachusetts Institute of Technology. 7, 18

**MSC** massive star cluster. 134

**MSP** millisecond pulsar. 25, 36

**NASA** the National Aeronautics and Space Administration. 10–12

**NRL** the Naval Research Laboratory. 18

**NS** neutron star. 18, 21, 34, 35, 39

**OG** outer gap. 39, 40

**OSO-3** the Third Orbiting Solar Observatory. xii, 9, 10

**PC** polar cap. 39

**PL** power law. 50

**PSF** point spread function. 16, 56, 135

**PWN** pulsar wind nebula. iv, v, xiv, xxv, 7, 19, 21, 23–26, 28, 29, 34, 38, 40–44, 51, 131, 132, 134–144

**SA** solid angle. 51, 52

**SAS-2** the second Small Astronomy Satellite. 10, 11

**SED** spectral energy distribution. xiii, 26, 27

**SN** supernova. 19, 21

**SNR** supernova remnant. 16, 24, 26, 38, 40, 41, 51

**TPC** two pole caustic. 39, 40

**UNID** unidentified source. 134, 135

**VHE** very high energy. ix, xi, xiii, 21, 26–28, 44, 131–142

## Chapter 9

# Population Study of LAT-detected PWNe

*This chapter is based the second part of the the paper “Constraints on the Galactic Population of TeV Pulsar Wind Nebulae using Fermi Large Area Telescope Observations” by Acero et al which is currently in prep.*

In Chapter 6, we search for new spatially-extended *Fermi* sources and found that spatial extension was an important characteristic for detecting new pulsar wind nebulae (PWNe). In the process, we discovered three new  $\gamma$ -ray emitting PWNs.

In Chapter 7, we then searched in the off-peak phase interval of the Large Area Telescope (LAT)-detected pulsars for new pulsar wind nebula and discovered 3C 58. Finally, in Chapter 8 we searched in the regions surrounding PWNs candidates detected at TeV energies for GeV-emitting PWNs 4 new PWNe candidates (HESS J1119–614, HESS J1303–631, HESS J1420–607, and HESS J1841–055) and 1 new PWN (HESS J1356–645)

In this chapter, we take the population of  $\gamma$ -ray emitting PWNs and PWNs candidates and study how thier multiwavlenth properties vary with propergies of the associated pulsar.

In Table 9.1, we compile the multiwavelenth properties of the very high energy (VHE) sources studied in Chapter 8. In particular, we include the spectrum observed at X-ray and VHE energies, the name of the associated pulsar, and the observed spin-down power, age, and distance of the pulsar.

Table 9.1. The muliwaveleth properties of the VHE source and their associated LAT-detected pulsars.

Source	$F_{1\text{ TeV}}^{30\text{ TeV}}$ ( $10^{-12}\text{ erg cm}^{-2}\text{ s}^{-1}$ )	$F_{2\text{ keV}}^{10\text{ keV}}$ ( $10^{-12}\text{ erg cm}^{-2}\text{ s}^{-1}$ )	PSR	$\dot{E}$ ( $\text{erg s}^{-1}$ )	$\tau$ (kyr)	Distance (kpc)
VER J0006+727	...	...	PSR J0007+7303	4.5e+35	13.9	$1.4 \pm 0.3$
Crab	$80 \pm 16$	$21000 \pm 4200$	PSR J0534+2200	4.6e+38	1.2	$2.0 \pm 0.5$
MGRO J0631+105	...	...	PSR J0631+1036	1.7e+35	43.6	$1.00 \pm 0.20$
MGRO J0632+17	...	...	PSR J0633+1746	3.2e+34	342	$0.2^{+0.2}_{-0.1}$
Vela-X	$79 \pm 21$	$54 \pm 11$	PSR J0835-4510	6.9e+36	11.3	$0.29 \pm 0.02$
HESS J1018-589	$0.9 \pm 0.4$	...	PSR J1016-5857	2.6e+36	21	3
HESS J1023-575	$4.8 \pm 1.7$	...	PSR J1023-5746	1.1e+37	4.6	2.8
HESS J1026-582	$5.9 \pm 4.4$	...	PSR J1028-5819	8.4e+35	90	$2.3 \pm 0.3$
HESS J1119-614	$2.3 \pm 1.2$	...	PSR J1119-6127	2.3e+36	1.6	$8.4 \pm 0.4$
HESS J1303-631	$27 \pm 1$	$0.16 \pm 0.03$	PSR J1301-6305	1.7e+36	11	$6.7^{+1.1}_{-1.2}$
HESS J1356-645	$6.7 \pm 3.7$	$0.06 \pm 0.01$	PSR J1357-6429	3.1e+36	7.3	$2.5^{+0.5}_{-0.4}$
HESS J1418-609	$3.4 \pm 1.8$	$3.1 \pm 0.1$	PSR J1418-6058	4.9e+36	1	$1.6 \pm 0.7$
HESS J1420-607	$15 \pm 3$	$1.3 \pm 0.3$	PSR J1420-6048	1.0e+37	13	$5.6 \pm 0.9$
HESS J1458-608	$3.9 \pm 2.4$	...	PSR J1459-6053	9.1e+35	64.7	4
HESS J1514-591	$20 \pm 4$	$29 \pm 6$	PSR J1513-5906	1.7e+37	1.56	$4.2 \pm 0.6$
HESS J1554-550	$1.6 \pm 0.5$	$3.1 \pm 1.0$	...	...	18	$7.8 \pm 1.3$
HESS J1616-508	$21 \pm 5$	$4.2 \pm 0.8$	PSR J1617-5055	1.6e+37	8.13	$6.8 \pm 0.7$
HESS J1632-478	$15 \pm 5$	$0.43 \pm 0.08$	...	3.0e+36	20	3
HESS J1640-465	$5.5 \pm 1.2$	$0.46 \pm 0.09$	...	4.0e+36	...	...
HESS J1646-458B	$5.0 \pm 2.0$	...	PSR J1648-4611	2.1e+35	110	$5.0 \pm 0.7$
HESS J1702-420	$9.0 \pm 3.0$	$0.01 \pm 0.00$	PSR J1702-4128	3.4e+35	55	$4.8 \pm 0.6$
HESS J1708-443	$23 \pm 7$	...	PSR J1709-4429	3.4e+36	17.5	$2.3 \pm 0.3$
HESS J1718-385	$4.3 \pm 1.6$	$0.14 \pm 0.03$	PSR J1718-3825	1.3e+36	89.5	$3.6 \pm 0.4$
HESS J1804-216	$12 \pm 2$	$0.07 \pm 0.01$	PSR J1803-2137	2.2e+36	16	$3.8^{+0.4}_{-0.5}$
HESS J1809-193	$19 \pm 6$	$0.23 \pm 0.05$	PSR J1809-1917	1.8e+36	51.3	$3.5 \pm 0.4$
HESS J1813-178	$5.0 \pm 0.6$	...	PSR J1813-1749	6.8e+37	5.4	4.7
HESS J1818-154	$1.3 \pm 0.9$	...	PSR J1818-1541	2.3e+33	9	$7.8^{+1.6}_{-1.4}$
HESS J1825-137	$61 \pm 14$	$0.44 \pm 0.09$	PSR J1826-1334	2.8e+36	21	$3.9 \pm 0.4$
HESS J1831-098	$5.1 \pm 0.6$	...	PSR J1831-0952	1.1e+36	128	$4.0 \pm 0.4$
HESS J1833-105	$2.4 \pm 1.2$	$40 \pm 0$	PSR J1833-1034	3.4e+37	4.85	$4.7 \pm 0.4$
HESS J1837-069	$23 \pm 9$	$0.64 \pm 0.24$	PSR J1836-0655	5.5e+36	2.23	$6.6 \pm 0.9$
HESS J1841-055	$23 \pm 3$	...	PSR J1838-0537	5.9e+36	4.97	1.3
HESS J1846-029	$9.0 \pm 1.5$	$29 \pm 1$	PSR J1846-0258	8.1e+36	0.73	5.1
HESS J1848-018	$4.3 \pm 1.0$	...	...	...	...	6
HESS J1849-000	$2.1 \pm 0.4$	$0.90 \pm 0.20$	PSR J1849-001	9.8e+36	42.9	7
HESS J1857+026	$18 \pm 3$	...	PSR J1856+0245	4.6e+36	20.6	$9.0 \pm 1.2$
MGRO J1908+06	$12 \pm 5$	...	PSR J1907+0602	2.8e+36	19.5	$3.2 \pm 0.3$
HESS J1912+101	$7.3 \pm 3.7$	...	PSR J1913+1011	2.9e+36	169	$4.8^{+0.5}_{-0.7}$
VER J1930+188	$2.3 \pm 1.3$	$5.2 \pm 0.1$	PSR J1930+1852	1.2e+37	2.89	$9^{+7}_{-2}$
VER J1959+208	...	...	PSR J1959+2048	1.6e+35	...	$2.5 \pm 1.0$
MGRO J2019+37	...	...	PSR J2021+3651	3.4e+36	17.2	$10^{+2}_{-4}$
MGRO J2228+61	...	$0.88 \pm 0.02$	PSR J2229+6114	2.2e+37	10.5	$0.80 \pm 0.20$

Note. — For the VHE PWN candidates, their multiwaveleth properties. This table includes the X-ray flux in the 1 TeV to 30 TeV energy range, the [INSERT MANUALLY]

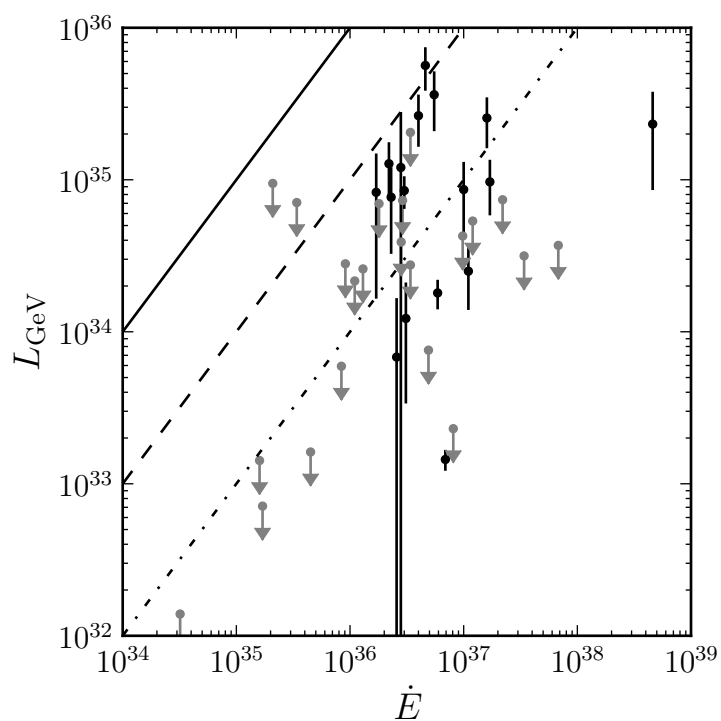


Figure 9.1 The observed  $\gamma$ -ray luminosity compared to the observed spin-down luminosity for all PWN candidates presented in Table 9.1.

In Figure 9.1, we compare the observed luminosity at GeV energies to the spin-down power of the observed pulsar. This plot shows that all LAT-detected PWNe emit a fraction  $\lesssim 10\%$  of their spin-down energy into powering the  $\gamma$ -ray emission from the pulsar wind.

Here we need to cite Mattana et al. (2009).

Next, we will discuss Figure 9.2. . .

Next, we will discuss Figure 9.3. . .

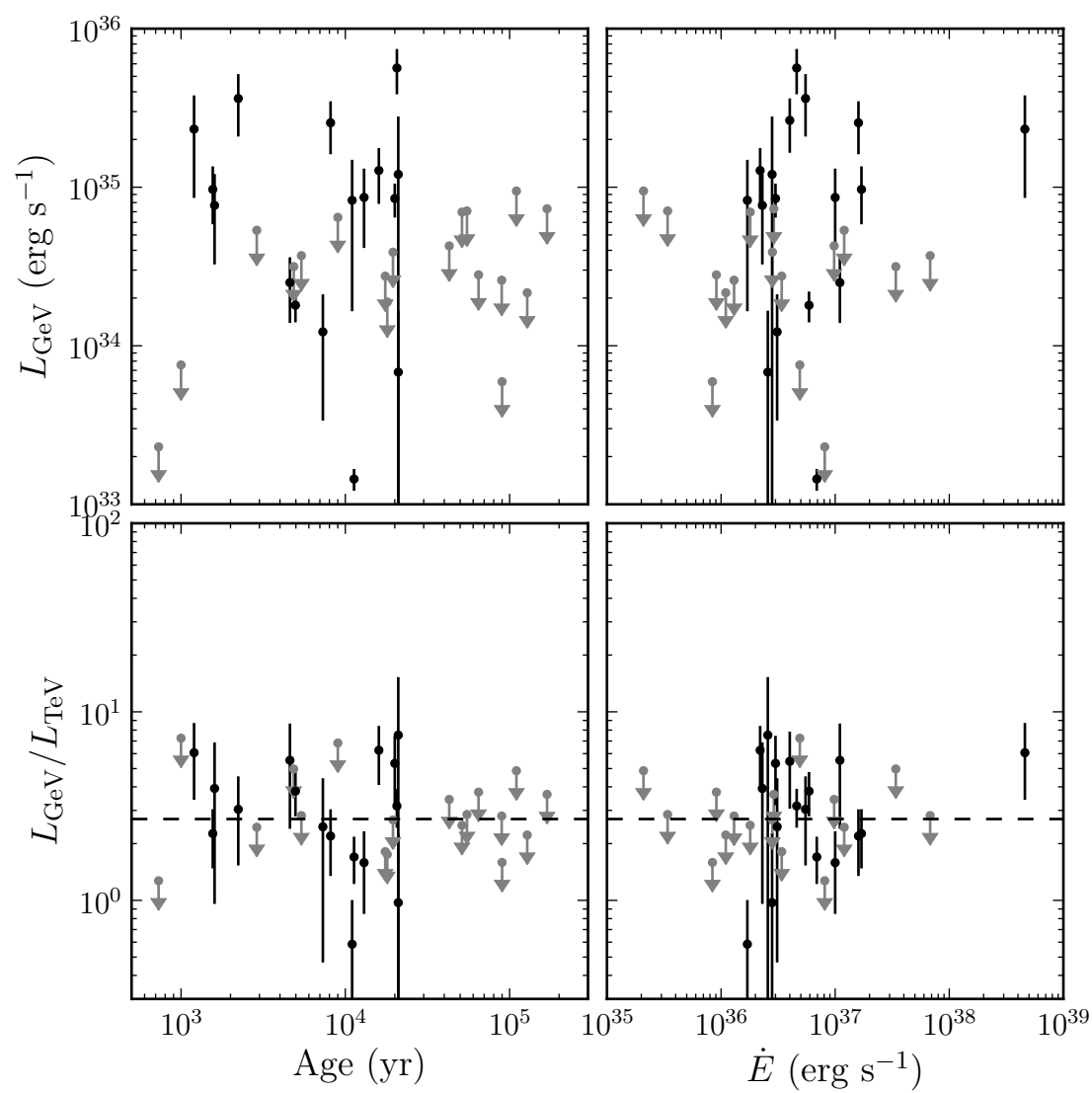


Figure 9.2 ...

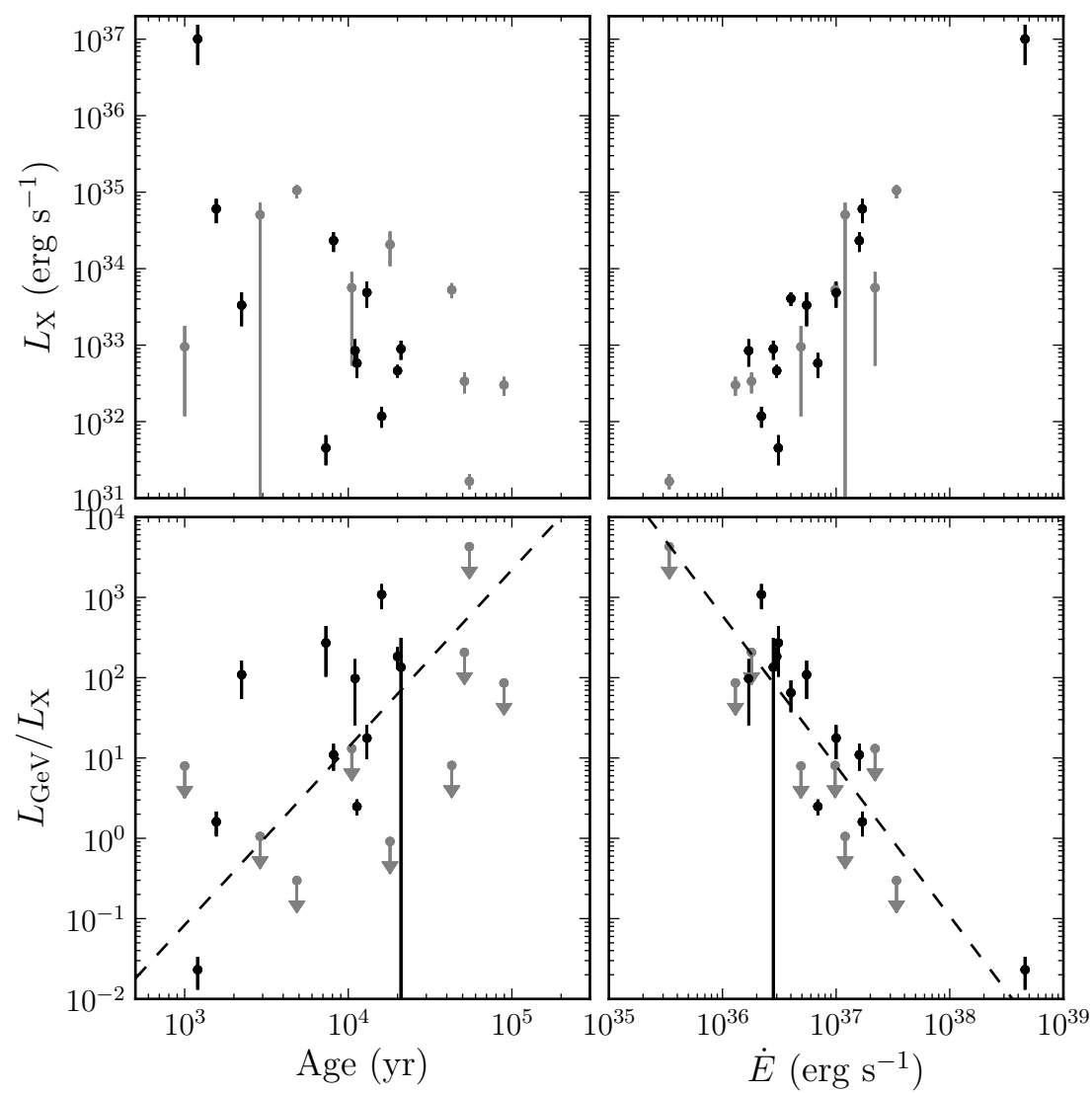


Figure 9.3 ...



# Bibliography

- Abdo, A., Ackermann, M., Ajello, M., et al. 2010, *Astrophys.J.*, 722, 1303
- Abdo, A. A., Ajello, M., Allafort, A., Baldini, L., & et al. in prep, *ApJS*
- Abdo, A. A., Allen, B., Berley, D., et al. 2007, *ApJ*, 664, L91
- Abdo, A. A., Ackermann, M., Ajello, M., et al. 2009a, *Physical Review Letters*, 103, 251101
- Abdo, A. A., Ackermann, M., Atwood, W. B., et al. 2009b, *ApJ*, 696, 1084
- Abdo, A. A., Ackermann, M., Ajello, M., et al. 2009c, *ApJ*, 706, L1
- . 2009d, *ApJS*, 183, 46
- Abdo, A. A., Allen, B. T., Aune, T., et al. 2009e, *ApJ*, 700, L127
- Abdo, A. A., Ackermann, M., Ajello, M., et al. 2009f, *Astroparticle Physics*, 32, 193
- . 2010a, *ApJ*, 714, 927
- Abdo, A. A., Ackermann, M., Ajello, M., et al. 2010b, *A&A*, 523, A46
- Abdo, A. A., Ackermann, M., Ajello, M., et al. 2010c, *Science*, 328, 725
- . 2010d, *ApJS*, 188, 405
- . 2010e, *ApJ*, 708, 1254
- . 2010f, *ApJ*, 718, 348

- Abdo, A. A., Ackermann, M., Ajello, M., et al. 2010, *The Astrophysical Journal*, 713, 146
- Abdo, A. A., Ackermann, M., Ajello, M., et al. 2010a, *Science*, 327, 1103
- . 2010b, *ApJ*, 712, 459
- Abdo, A. A., Ackermann, M., Ajello, M., et al. 2010c, *A&A*, 512, A7
- Abdo, A. A., Ackermann, M., Ajello, M., et al. 2010d, *Physical Review Letters*, 104, 101101
- . 2010e, *ApJS*, 187, 460
- . 2011a, *Science*, 331, 739
- . 2011b, *ApJ*, 734, 28
- Acciari, V. A., Aliu, E., Arlen, T., et al. 2009, *ApJ*, 698, L133
- . 2010, *ApJ*, 719, L69
- . 2011, *ApJ*, 738, 3
- Acero, F., Ackermann, M., Ajello, M., & et al. in prep., *ApJ*
- Acero, F., Djannati-Ataï, A., Förster, A., et al. 2012, *ArXiv e-prints*
- Ackermann, M., Ajello, M., Allafort, A., et al. in prep, *ApJ*
- Ackermann, M., Ajello, M., Baldini, L., et al. 2011a, *ApJ*, 726, 35
- Ackermann, M., Ajello, M., Allafort, A., et al. 2011b, *ApJ*, 743, 171
- Ackermann, M., Ajello, M., Atwood, W. B., et al. 2012, *The Astrophysical Journal*, 750, 3
- Ackermann, M., Ajello, M., Albert, A., et al. 2012, *ApJS*, 203, 4
- Aharonian, F., Akhperjanian, A. G., Aye, K.-M., et al. 2005a, *A&A*, 435, L17

—. 2005b, *A&A*, 439, 1013

Aharonian, F., Akhperjanian, A. G., Bazer-Bachi, A. R., et al. 2006a, *A&A*, 460, 743

—. 2006b, *A&A*, 456, 245

—. 2006c, *A&A*, 460, 365

—. 2006d, *A&A*, 448, L43

—. 2006e, *ApJ*, 636, 777

—. 2007a, *A&A*, 467, 1075

—. 2007b, *A&A*, 472, 489

—. 2007c, *ApJ*, 661, 236

—. 2007d, *A&A*, 464, 235

—. 2008a, *A&A*, 481, 401

Aharonian, F., Akhperjanian, A. G., Barres de Almeida, U., et al. 2008b, *A&A*, 484, 435

—. 2008c, *A&A*, 477, 353

Aharonian, F., Akhperjanian, A. G., Anton, G., et al. 2009, *A&A*, 499, 723

Aharonian, F. A., & Bogovalov, S. V. 2003, *New A*, 8, 85

Aharonian, F. A., Coppi, P. S., & Voelk, H. J. 1994, *ApJ*, 423, L5

Aharonian, F. A., Akhperjanian, A. G., Bazer-Bachi, A. R., et al. 2005c, *A&A*, 442, L25

—. 2007e, *A&A*, 469, L1

Ajello, M., Allafort, A., Baldini, L., et al. 2012, *ApJ*, 744, 80

- Akaike, H. 1974, IEEE Transactions on Automatic Control, 19, 716
- Albert, J., Aliu, E., Anderhub, H., et al. 2006, Science, 312, 1771
- Aliu, E. 2011, in International Cosmic Ray Conference, Vol. 7, International Cosmic Ray Conference, 227
- Arnold, J. R., Metzger, A. E., Anderson, E. C., & van Dilla, M. A. 1962, J. Geophys. Res., 67, 4878
- Arons, J. 1996, Space Sci. Rev., 75, 235
- Ashworth, William B., J. 1981, Proceedings of the American Philosophical Society, 125, pp. 52
- Atwood, W. B., Abdo, A. A., Ackermann, M., et al. 2009, ApJ, 697, 1071
- Baade, W., & Zwicky, F. 1934, Physical Review, 46, 76
- Balbo, M., Saouter, P., Walter, R., et al. 2010, A&A, 520, A111
- Baltz, E. A., Berenji, B., Bertone, G., et al. 2008, J. Cosmology Astropart. Phys., 7, 13
- Bamba, A., Ueno, M., Koyama, K., & Yamauchi, S. 2003, The Astrophysical Journal, 589, 253
- Bartoli, B., Bernardini, P., Bi, X. J., et al. 2012, ApJ, 745, L22
- Baum, W. A., Johnson, F. S., Oberly, J. J., et al. 1946, Phys. Rev., 70, 781
- Bertsch, D. L., Brazier, K. T. S., Fichtel, C. E., et al. 1992, Nature, 357, 306
- Bignami, G. F., Boella, G., Burger, J. J., et al. 1975, Space Science Instrumentation, 1, 245
- Blandford, R. D., & Romani, R. W. 1988, MNRAS, 234, 57P
- Blumenthal, G. R., & Gould, R. J. 1970, Rev. Mod. Phys., 42, 237

- Bogovalov, S. V., & Aharonian, F. A. 2000, *MNRAS*, 313, 504
- Bolton, J. G., Stanley, G. J., & Slee, O. B. 1949, *Nature*, 164, 101
- Bowyer, S., Byram, E. T., Chubb, T. A., & Friedman, H. 1964, *Science*, 146, 912
- Bradt, H., Rappaport, S., & Mayer, W. 1969, *Nature*, 222, 728
- Browning, R., Ramsden, D., & Wright, P. J. 1971, *Nature Physical Science*, 232, 99
- Brumfiel, G. 2007, *Nature*, 448, 974
- Buehler, R., Scargle, J. D., Blandford, R. D., et al. 2012, *ApJ*, 749, 26
- Burnham, K. P., & Anderson, D. R. 2002, *Model selection and multimodel inference: a practical information-theoretic approach*, 2nd edn. (Springer)
- Burnight, T. 1949, *Phys. Rev*, 76, 19
- Caballero, I., & Wilms, J. 2012, *Mem. Soc. Astron. Italiana*, 83, 230
- Carroll, B. W., & Ostlie, D. A. 2006, *An Introduction to Modern Astrophysics*, 2nd edn. (Benjamin Cummings)
- Cash, W. 1979, *ApJ*, 228, 939
- Castelletti, G., Dubner, G., Golap, K., & Goss, W. M. 2006, *A&A*, 459, 535
- Caswell, J. L., Milne, D. K., & Wellington, K. J. 1981, *MNRAS*, 195, 89
- Chandrasekhar, S. 1931, *ApJ*, 74, 81
- Chaves, R. C. G., Renaud, M., Lemoine-Goumard, M., & Goret, P. 2008, in *American Institute of Physics Conference Series*, Vol. 1085, American Institute of Physics Conference Series, ed. F. A. Aharonian, W. Hofmann, & F. Rieger, 372–375
- Chen, A. W., Piano, G., Tavani, M., et al. 2011, *A&A*, 525, A33
- Cheng, K. S., Ho, C., & Ruderman, M. 1986, *ApJ*, 300, 522

- Clifton, T. R., Lyne, A. G., Jones, A. W., McKenna, J., & Ashworth, M. 1992, MNRAS, 254, 177
- Cocke, W. J., Disney, M. J., & Taylor, D. J. 1969, Nature, 221, 525
- Collins, II, G. W., Claspy, W. P., & Martin, J. C. 1999, PASP, 111, 871
- Critchfield, C. L., Ney, E. P., & Oleksa, S. 1952, Physical Review, 85, 461
- Dame, T. M. 2011, ArXiv e-prints
- Daugherty, J. K., & Harding, A. K. 1996, ApJ, 458, 278
- de Geus, E. J., Bronfman, L., & Thaddeus, P. 1990, A&A, 231, 137
- de Jager, O. C., & Djannati-Ataï, A. 2009, in Astrophysics and Space Science Library, Vol. 357, Astrophysics and Space Science Library, ed. W. Becker, 451
- de Jager, O. C., Raubenheimer, B. C., & Swanepoel, J. W. H. 1989, A&A, 221, 180
- de los Reyes, R., Zajczyk, A., Chaves, R. C. G., & for the H. E. S. S. collaboration. 2012, ArXiv e-prints
- de Naurois, M., & H.E.S.S. Collaboration. 2013, Advances in Space Research, 51, 258
- Demorest, P. B., Pennucci, T., Ransom, S. M., Roberts, M. S. E., & Hessels, J. W. T. 2010, Nature, 467, 1081
- Djannati-Ataï, A., de Jager, O. C., Terrier, R., & et al. 2008, in International Cosmic Ray Conference, Vol. 2, International Cosmic Ray Conference, 823–826
- Domainko, W., & Ohm, S. 2012, A&A, 545, A94
- Dombrovsky, V. A. 1954, Doklady Akademiyi Nauk USSR, 94, 1021
- Duncan, J. C. 1921, Proceedings of the National Academy of Science, 7, 179
- Dyks, J., & Rudak, B. 2003, ApJ, 598, 1201

- Eadie, W. T., Drijard, D., & James, F. E. 1971, *Statistical methods in experimental physics* (North-Holland Pub. Co.)
- Espinoza, C. M., Lyne, A. G., Kramer, M., Manchester, R. N., & Kaspi, V. M. 2011, *ApJ*, 741, L13
- Esposito, J. A., Bertsch, D. L., Chen, A. W., et al. 1999, *ApJS*, 123, 203
- Falanga, M., Kuiper, L., Poutanen, J., et al. 2005, *A&A*, 444, 15
- Feenberg, E., & Primakoff, H. 1948, *Phys. Rev.*, 73, 449
- Fichtel, C. E., Hartman, R. C., Kniffen, D. A., et al. 1975, *ApJ*, 198, 163
- Finley, J. P., Srinivasan, R., & Park, S. 1996, *ApJ*, 466, 938
- Fisher, R. A. 1925, *Statistical Methods for Research Workers* (Edinburgh: Oliver and Boyd)
- Fritz, G., Henry, R. C., Meekins, J. F., Chubb, T. A., & Friedman, H. 1969, *Science*, 164, 709
- Funk, S., Hinton, J. A., Pühlhofer, G., et al. 2007, *ApJ*, 662, 517
- Gaensler, B. M., Schulz, N. S., Kaspi, V. M., Pivovarov, M. J., & Becker, W. E. 2003, *ApJ*, 588, 441
- Gaensler, B. M., & Slane, P. O. 2006, *ARA&A*, 44, 17
- Gaisser, T. K., Protheroe, R. J., & Stanev, T. 1998, *ApJ*, 492, 219
- Gelfand, J. D., Slane, P. O., & Zhang, W. 2009, *ApJ*, 703, 2051
- Giordano, F., & Fermi LAT Collaboration. 2011, in *High-Energy Emission from Pulsars and their Systems*, ed. D. F. Torres & N. Rea, 69
- Gold, T. 1968, *Nature*, 218, 731
- Goldreich, P., & Julian, W. H. 1969, *ApJ*, 157, 869

- Górski, K. M., Hivon, E., Banday, A. J., et al. 2005, *ApJ*, 622, 759
- Gotthelf, E. V., & Halpern, J. P. 2008, *ApJ*, 681, 515
- Gould, R. J., & Burbidge, G. R. 1965, *Annales d'Astrophysique*, 28, 171
- Grenier, I. A., Casandjian, J.-M., & Terrier, R. 2005, *Science*, 307, 1292
- Grindlay, J. E., & Hoffman, J. A. 1971, *Astrophys. Lett.*, 8, 209
- Grondin, M.-H., Funk, S., Lemoine-Goumard, M., et al. 2011, *ApJ*, 738, 42
- Gunn, J. E., & Ostriker, J. P. 1969, *Nature*, 221, 454
- H. E. S. S. Collaboration, Abramowski, A., Acero, F., et al. 2012, *A&A*, 541, A5
- Hall, T. A., Bond, I. H., Bradbury, S. M., et al. 2003, *ApJ*, 583, 853
- Hartman, R. C., Bertsch, D. L., Bloom, S. D., et al. 1999, *ApJS*, 123, 79
- Haug, E. 1975, *Zeitschrift Naturforschung Teil A*, 30, 1099
- . 1997, *A&A*, 326, 417
- Hayakawa, S. 1952, *Progress of Theoretical Physics*, 8, 571
- Heitler, W. 1954, *The Quantum Theory of Radiation*, Dover Books on Physics Series (New York : Dover Publications, Incorporated)
- Herschel, W. 1800, *Philosophical Transactions of the Royal Society of London*, 90, pp. 284
- H.E.S.S. Collaboration, Abramowski, A., Acero, F., et al. 2011a, *A&A*, 531, A81
- . 2011b, *A&A*, 528, A143
- H.E.S.S. Collaboration, Acero, F., Aharonian, F., et al. 2011c, *A&A*, 525, A45
- H.E.S.S. Collaboration, Abramowski, A., Acero, F., et al. 2011d, *A&A*, 533, A103



—. 2011e, *A&A*, 525, A46

Hessels, J. W. T., Nice, D. J., Gaensler, B. M., et al. 2008, *ApJ*, 682, L41

Hester, J. J. 2008, *ARA&A*, 46, 127

Hewish, A., Bell, S. J., Pilkington, J. D. H., Scott, P. F., & Collins, R. A. 1968, *Nature*, 217, 709

Hewitt, J., Grondin, M.-H., Lemoine-Goumard, M., et al. 2012

Hofverberg, P. 2011, in *International Cosmic Ray Conference*, Vol. 7, *International Cosmic Ray Conference*, 247

Hoppe, S. 2008, in *International Cosmic Ray Conference*, Vol. 2, *International Cosmic Ray Conference*, 579–582

Houck, J. C., & Allen, G. E. 2006, *ApJS*, 167, 26

Hulsizer, R. I., & Rossi, B. 1948, *Phys. Rev.*, 73, 1402

Hutchinson, G. 1952, *Philosophical Magazine Series 7*, 43, 847

Hwang, U., Petre, R., & Flanagan, K. A. 2008, *ApJ*, 676, 378

James, F., & Roos, M. 1975, *Computer Physics Communications*, 10, 343

Jansky, K. 1933, *Proceedings of the Institute of Radio Engineers*, 21, 1387

Kamae, T., Karlsson, N., Mizuno, T., Abe, T., & Koi, T. 2006, *ApJ*, 647, 692

Kargaltsev, O., Pavlov, G. G., & Wong, J. A. 2008, *ArXiv e-prints*

Kaspi, V. M., & Helfand, D. J. 2002, in *Astronomical Society of the Pacific Conference Series*, Vol. 271, *Neutron Stars in Supernova Remnants*, ed. P. O. Slane & B. M. Gaensler, 3

Kaspi, V. M., Roberts, M. S. E., & Harding, A. K. 2006, *Isolated neutron stars*, ed. W. H. G. Lewin & M. van der Klis, 279–339

- Katagiri, H., Tibaldo, L., Ballet, J., et al. 2011, *ApJ*, 741, 44
- Katsuta, J., Uchiyama, Y., Tanaka, T., et al. 2012
- Kennel, C. F., & Coroniti, F. V. 1984a, *ApJ*, 283, 694
- . 1984b, *ApJ*, 283, 710
- Kerr, M. 2010, PhD thesis, University of Washington
- Kijak, J., & Gil, J. 2003, *A&A*, 397, 969
- King, I. 1962, *AJ*, 67, 471
- Klein, O., & Nishina, T. 1929, *Zeitschrift fur Physik*, 52, 853
- Kniffen, D. A., & Fichtel, C. E. 1970, *ApJ*, 161, L157
- Koch, H. W., & Motz, J. W. 1959, *Reviews of Modern Physics*, 31, 920
- Krause, J., Carmona, E., Reichardt, I., & for the MAGIC Collaboration. 2011, *ArXiv e-prints*
- Kraushaar, W., Clark, G. W., Garmire, G., et al. 1965, *ApJ*, 141, 845
- Kraushaar, W. L., Clark, G. W., Garmire, G. P., et al. 1972, *ApJ*, 177, 341
- Lampland, C. O. 1921, *PASP*, 33, 79
- Lande, J., Ackermann, M., Allafort, A., et al. 2012
- Landi, R., de Rosa, A., Dean, A. J., et al. 2007a, *MNRAS*, 380, 926
- Landi, R., Masetti, N., Bassani, L., et al. 2007b, *The Astronomer's Telegram*, 1047, 1
- Large, M. I., Vaughan, A. E., & Mills, B. Y. 1968, *Nature*, 220, 340
- Lemoine-Goumard, M., Ferrara, E., Grondin, M.-H., Martin, P., & Renaud, M. 2011, *Mem. Soc. Astron. Italiana*, 82, 739

- Li, T.-P., & Ma, Y.-Q. 1983, *ApJ*, 272, 317
- Longair, M. S. 2011, *High Energy Astrophysics*, 3rd edn. (The Edinburgh Building, Cambridge CB2 8RU, UK: Cambridge University Press)
- Lundmark, K. 1921, *PASP*, 33, 225
- Manchester, R. N., Hobbs, G. B., Teoh, A., & Hobbs, M. 2005, *AJ*, 129, 1993
- Markwardt, C. B., & Ogelman, H. 1995, *Nature*, 375, 40
- Matsumoto, H., Ueno, M., Bamba, A., et al. 2007, *PASJ*, 59, 199
- Matsumoto, H., Uchiyama, H., Sawada, M., et al. 2008, *PASJ*, 60, 163
- Mattana, F., Falanga, M., Götz, D., et al. 2009, *ApJ*, 694, 12
- Mattox, J. R., Bertsch, D. L., Fichtel, C. E., et al. 1992, *ApJ*, 401, L23
- Mattox, J. R., Bertsch, D. L., Chiang, J., et al. 1996, *ApJ*, 461, 396
- Mayall, N. U., & Oort, J. H. 1942, *PASP*, 54, 95
- Mayer-Hasselwander, H. A., Kanbach, G., Bennett, K., et al. 1982, *A&A*, 105, 164
- McArthur, S. 2011, *ArXiv e-prints*
- McK Mahille, J., Schild, R., Wendorf, F., & Brenner, R. 2007, *African Skies*, 11, 2
- Meegan, C., Lichti, G., Bhat, P. N., et al. 2009, *ApJ*, 702, 791
- Mizukami, T., Kubo, H., Yoshida, T., et al. 2011, *ApJ*, 740, 78
- Morrison, P. 1958, *Il Nuovo Cimento*, 7, 858
- Moskalenko, I. V., & Strong, A. W. 2000, *ApJ*, 528, 357
- Murphy, T., Mauch, T., Green, A., et al. 2007, *MNRAS*, 382, 382
- Muslimov, A. G., & Harding, A. K. 2004, *ApJ*, 606, 1143

- Neronov, A., Semikoz, D. V., Tinyakov, P. G., & Tkachev, I. I. 2011, *A&A*, 526, A90
- Nolan, P. L., Arzoumanian, Z., Bertsch, D. L., et al. 1993, *ApJ*, 409, 697
- Nolan, P. L., Fierro, J. M., Lin, Y. C., et al. 1996, *A&AS*, 120, C61
- Nolan, P. L., Abdo, A. A., Ackermann, M., et al. 2012, *ApJS*, 199, 31
- Pacini, F. 1967, *Nature*, 216, 567
- . 1968, *Nature*, 219, 145
- Pacini, F., & Salvati, M. 1973, *ApJ*, 186, 249
- Paron, S., Dubner, G., Reynoso, E., & Rubio, M. 2008, *A&A*, 480, 439
- Pellizzoni, A., Trois, A., Tavani, M., et al. 2010, *Science*, 327, 663
- Petre, R., Becker, C. M., & Winkler, P. F. 1996, *The Astrophysical Journal Letters*, 465, L43
- Pittori, C., & the AGILE Team. 2003, *Chinese Journal of Astronomy and Astrophysics*, 3, 517
- Pollock, A. M. T. 1985, *A&A*, 150, 339
- Protassov, R., van Dyk, D. A., Connors, A., Kashyap, V. L., & Siemiginowska, A. 2002, *ApJ*, 571, 545
- Rea, N., & Esposito, P. 2011, in *High-Energy Emission from Pulsars and their Systems*, ed. D. F. Torres & N. Rea, 247
- Rees, M. J., & Gunn, J. E. 1974, *MNRAS*, 167, 1
- Renaud, M., Goret, P., & Chaves, R. C. G. 2008, in *American Institute of Physics Conference Series*, Vol. 1085, American Institute of Physics Conference Series, ed. F. A. Aharonian, W. Hofmann, & F. Rieger, 281–284
- Reynoso, E. M., Dubner, G. M., Goss, W. M., & Arnal, E. M. 1995, *AJ*, 110, 318

- Reynoso, E. M., Green, A. J., Johnston, S., et al. 2003, MNRAS, 345, 671
- Richards, D. W., & Comella, J. M. 1969, Nature, 222, 551
- Rieke, G. H., & Weekes, T. C. 1969, ApJ, 155, 429
- Rishbeth, H. 1958, Australian Journal of Physics, 11, 550
- Rodriguez, J., Tomsick, J. A., Foschini, L., et al. 2003, A&A, 407, L41
- Romani, R. W. 1996, ApJ, 470, 469
- Romani, R. W., Kerr, M., Craig, H. A., et al. 2011, ApJ, 738, 114
- Rousseau, R., Grondin, M.-H., Van Etten, A., et al. 2012, A&A, 544, A3
- Rowell, G., Horns, D., Fukui, Y., & Moriguchi, Y. 2008, in American Institute of Physics Conference Series, Vol. 1085, American Institute of Physics Conference Series, ed. F. A. Aharonian, W. Hofmann, & F. Rieger, 241–244
- Rybicki, G. B., & Lightman, A. P. 1979, Radiative processes in astrophysics (New York: John Wiley & Sons Ltd)
- Schwarz, G. 1978, The Annals of Statistics, 6, pp. 461
- Seward, F. D., & Harnden, Jr., F. R. 1982, ApJ, 256, L45
- Shaver, P. A., & Goss, W. M. 1970, Australian Journal of Physics Astrophysical Supplement, 14, 133
- Sheidaei, F. 2011, in International Cosmic Ray Conference, Vol. 7, International Cosmic Ray Conference, 243
- Shklovskii, I. S. 1953, Doklady Akad. Nauk SSSR, 90, 983
- Slane, P., Castro, D., Funk, S., et al. 2010, The Astrophysical Journal, 720, 266
- Slane, P., Castro, D., Funk, S., et al. 2010, ApJ, 720, 266

- Slane, P., Helfand, D. J., van der Swaluw, E., & Murray, S. S. 2004, *ApJ*, 616, 403
- Sreekumar, P., Bertsch, D. L., Hartman, R. C., Nolan, P. L., & Thompson, D. J. 1999, *Astroparticle Physics*, 11, 221
- Sreekumar, P., Bertsch, D. L., Dingus, B. L., et al. 1992, *ApJ*, 400, L67
- Sreekumar, P., Bertsch, D. L., Dingus, B. L., et al. 1998, *The Astrophysical Journal*, 494, 523
- Staelin, D. H., & Reifenstein, III, E. C. 1968, *Science*, 162, 1481
- Strong, A. W., & Moskalenko, I. V. 1998, *ApJ*, 509, 212
- Sugizaki, M., Mitsuda, K., Kaneda, H., et al. 2001, *ApJS*, 134, 77
- Swanenburg, B. N., Hermsen, W., Bennett, K., et al. 1978, *Nature*, 275, 298
- Swanenburg, B. N., Bennett, K., Bignami, G. F., et al. 1981, *ApJ*, 243, L69
- Tam, P. H. T., Wagner, S. J., Tibolla, O., & Chaves, R. C. G. 2010, *A&A*, 518, A8
- Tanaka, T., Allafort, A., Ballet, J., et al. 2011, *ApJ*, 740, L51
- Taylor, A. R., Gibson, S. J., Peracaula, M., et al. 2003, *AJ*, 125, 3145
- Terrier, R., Mattana, F., Djannati-Atai, A., et al. 2008, in *American Institute of Physics Conference Series*, Vol. 1085, *American Institute of Physics Conference Series*, ed. F. A. Aharonian, W. Hofmann, & F. Rieger, 312–315
- The Fermi LAT Collaboration, Coe, M. J., Di Mille, F., et al. 2012, *ArXiv e-prints*
- Thompson, D. J. 2008, *Reports on Progress in Physics*, 71, 116901
- Thompson, D. J., Fichtel, C. E., Hartman, R. C., Kniffen, D. A., & Lamb, R. C. 1977a, *ApJ*, 213, 252
- Thompson, D. J., Fichtel, C. E., Kniffen, D. A., & Ogelman, H. B. 1977b, *ApJ*, 214, L17

- Thompson, D. J., Bertsch, D. L., Fichtel, C. E., et al. 1993, *ApJS*, 86, 629
- Tomsick, J. A., Lingenfelter, R., Walter, R., et al. 2003, *IAU Circ.*, 8076, 1
- Torii, K., Kinugasa, K., Toneri, T., et al. 1998, *ApJ*, 494, L207
- Trussoni, E., Massaglia, S., Caucino, S., Brinkmann, W., & Aschenbach, B. 1996, *A&A*, 306, 581
- van der Swaluw, E., & Wu, Y. 2001, *ApJ*, 555, L49
- Vladimirov, A. E., Digel, S. W., Jóhannesson, G., et al. 2011, *Computer Physics Communications*, 182, 1156
- Watters, K. P., & Romani, R. W. 2011, *ApJ*, 727, 123
- Weekes, T. C., Cawley, M. F., Fegan, D. J., et al. 1989, *ApJ*, 342, 379
- Weinstein, A., & for the VERITAS Collaboration. 2009, *ArXiv e-prints*
- Wilks, S. S. 1938, *Annals of Mathematical Statistics*, 9, 60
- Young, E. T., Lada, C. J., & Wilking, B. A. 1986, *ApJ*, 304, L45